Materials Today Communications 26 (2021) 102133

Contents lists available at ScienceDirect

Materials Today Communications

journal homepage: www.elsevier.com/locate/mtcomm

Enhanced sulfur utilization in lithium-sulfur batteries by hybrid modified separators

Lei Zhou [a,b], Hao Li [c], Yue Zhang [a], Ming Jiang [a,b], Dmitri L. Danilov [a,b], Rüdiger-A. Eichel [b,d], Peter H.L. Notten [a,b,e,*]

[a] Eindhoven University of Technology, P.O. Box 513, 5600 MB, Eindhoven, the Netherlands
[b] Institute of Energy and Climate Research, Fundamental Electrochemistry (IEK-9), Forschungszentrum Jülich, D-52425, Jülich, Germany
[c] Center for Biomedical Optics and Photonics (CBOP) & College of Physics and Optoelectronic Engineering, Key Laboratory of Optoelectronic Devices and Systems, Shenzhen University, Shenzhen, 518060, PR China
[d] Institute of Physical Chemistry, RWTH Aachen University, D-52074, Aachen, Germany
[e] Centre for Clean Energy Technology, University of Technology Sydney, Broadway, Sydney, NSW, 2007, Australia

ARTICLE INFO

Keywords:
Li-S battery
Polysulfide
Carbon nanotube
Layered double hydroxide
Chemical bonding

ABSTRACT

The extraordinary energy density and low cost enable lithium-sulfur (Li-S) batteries to be a promising alternative to traditional energy storage systems. The principal hurdle facing Li-S batteries is the unsatisfactory utilization of sulfur cathodes. The detrimental shuttle issue of polysulfides and the sluggish charge transfer kinetics result in quick capacity degradation of Li-S batteries. An MFLC hybrid material composed of manganese-iron layered double hydroxides (Mn-Fe LDH) and carbon nanotubes (CNT) has been developed. Such heterostructure combines the advantages of effective chemical bonding of Mn-Fe LDH towards polysulfides with the high conductivity of CNT. When modified on a polypropylene (PP) separator, the hybrid material is proven to significantly inhibit the shuttle issue of polysulfides and accelerate their redox reaction kinetics. Li-S batteries with MFLC-modified separators revealed considerably improved electrochemical performance. A high initial capacity of 1138 mA h g^{-1} and 70 % capacity retention after 200 cycles were achieved at 0.2 C. The enhanced sulfur utilization can be directly evaluated from the discharge voltage plateaus. The results indicate a new solution for the practical application of Li-S batteries and provide a simple approach to determine the efficiency of sulfur utilization.

1. Introduction

The emergence of clean and sustainable energy storage systems significantly reduces the current dependence on traditional fossil fuels, such as coal, oil, and natural gas. Lithium-ion batteries have been proven to be an effective solution to store electricity generated from other power sources [1,2]. Due to the limited energy density, current lithium-ion battery technologies face challenges to satisfy the increasing application scenarios, such as electric vehicles and stationary storage systems. Lithium-sulfur (Li-S) batteries are gaining attention because of the high theoretical energy density of 2600 Wh kg^{-1} [3–6]. Li-S batteries are expected to be a promising solution for future energy storage challenges. Moreover, the high abundance of sulfur makes Li-S batteries very attractive for low-cost applications.

However, the complicated electrochemistry of sulfur cathodes incurs a relatively poor battery performance. The insulating nature of sulfur and its final discharge products aggravate the redox kinetics of sulfur cathodes [7]. In addition, soluble polysulfide intermediates produced during cycling are prone to diffuse into the electrolyte, leading to severe capacity losses [8]. As a result, sulfur can hardly be fully utilized. Substantial scientific endeavors have been made to explore conductive carbon structures to enhance the conductivity of sulfur cathodes [9–13]. Besides, polar metal compounds have been proven to effectively anchor polysulfides by forming chemical bonds to prevent the loss of active sulfur species [14,15]. One of the most effective strategies is to modify the separators by polar metal compounds, by which polysulfides can be restricted within the cathode side [16–18]. Such polysulfide barriers improve the electrochemical performance of Li-S batteries. Thorough understanding and evaluation of their function and role in regulating sulfur utilization will therefore facilitate the design of more advanced

* Corresponding author at: Eindhoven University of Technology, P.O. Box 513, 5600 MB, Eindhoven, the Netherlands.
E-mail address: p.h.l.notten@tue.nl (P.H.L. Notten).

https://doi.org/10.1016/j.mtcomm.2021.102133
Received 22 October 2020; Received in revised form 2 February 2021; Accepted 2 February 2021
Available online 12 February 2021

sulfur cathodes.

Highly conductive CNT enable good electron transport in sulfur cathodes [19–21]. The improved conductivity helps mitigate battery polarization and increase the (dis)charge ability at high current densities. However, CNT cannot adequately confine the polysulfides in the cathodes due to its weak sulfur adsorption properties. On the other hand, polar metal compounds are frequently used to prevent the loss of sulfur species from cathodes. Some of these materials, such as Ti_4O_7 [22–24], Co_3O_4 [25–27], TiS_2 [28,29], and MXenes [30–32], display improved chemical adsorption towards polysulfides via polar-polar or Lewis acid-base interaction. The shuttle issue can be significantly alleviated by these materials. Other materials, including MnO_2 [33], MoS_2 [34], and CoS_2 [35], can catalyze and mediate the conversion of sulfur species during battery cycling, thus improving the redox kinetics of sulfur cathodes. Among them, layered double hydroxides (LDH) with abundant surface sites combine good polysulfide adsorption with enhanced redox kinetics of sulfur cathodes [36,37]. Therefore, the dual advantages of CNT and LDH are beneficial for sulfur utilization and, consequently, to improve the electrochemical performance of Li-S batteries.

Herein, a manganese-iron layered double hydroxide (Mn-Fe LDH), *in-situ* grown on CNT, is reported. Hybrid composite materials, denoted as MFLC, have been single-sided deposited on polypropylene (PP) separators, acting as an effective barrier for polysulfides (Fig. 1a). Such modification may significantly increase the electrochemical performance of Li-S batteries by enhancing sulfur utilization. The dense modification layer serves as a physical barrier to block the shuttling of polysulfides. As schematically shown in Fig. 1b, the Mn-Fe LDH nanosheets grown *in-situ* on the CNT offer abundant polar sites to chemically anchor polysulfides and also accelerate their electrochemical conversion kinetics. Besides, the modification layer can also act as an additional current collector to facilitate electron transport due to the good conductivity of CNT. Li-S batteries with an MFLC-modified separator benefit from these advantages and have achieved a high discharge capacity of 1138 mA h g^{-1} and enhanced redox kinetics. Therefore, such MFLC modification layers are to be expected to play an essential role in the practical application of future Li-S batteries.

2. Experimental

2.1. Synthesis of MFLC hybrid materials

All chemicals were purchased from Sigma Aldrich and directly used without further purification. MFLC was synthesized using a co-precipitation method. 1.0 mg mL^{-1} oxidized CNT aqueous solutions were ultrasonicated for 2 h to achieve a good dispersion. Then 10 mL of 30 mM $MnCl_2$ and 10 mM $FeCl_3$ aqueous solution were added into CNT under stirring. Subsequently, 0.15 M NaOH aqueous solution (40 mL) was quickly poured into the mixture and vigorously stirred for 90 min. After that, the MFLC hybrid material was collected by centrifuge separation. The obtained slurry was dispersed in 35 mL distilled water for a hydrothermal reaction at 120 °C for 16 h. The final product was collected after centrifuging and washing with distilled water. Pure Mn-Fe LDH was synthesized via a similar procedure without adding CNT.

2.2. Fabrication of modified separators

MFLC-modified separators were fabricated by coating an MFLC slurry on the Celgard 2400 PP separator via a doctor blade method. 90 wt.% MFLC was mixed with 10 wt.% poly(vinylidene fluoride) (PVDF) binder and then dispersed in N-methyl pyrrolidone (NMP) solvent by stirring. The obtained slurry was coated on a PP separator and then dried overnight at 50 °C. The deposited amount on the separator was controlled to be about 0.5 mg cm^{-2}. Finally, MFLC-modified separators were punched into disks with a diameter of 16 mm for assembling cells. CNT-modified separators were fabricated with the same method by coating CNT on the PP separator.

2.3. Fabrication of sulfur cathodes

Sulfur/carbon (S/C) composites were fabricated by a melt-diffusion method. Pure sulfur was mixed with commercial carbon black (CB) in a mass ratio of S:C = 7:3 at 155 °C for 12 h. The sulfur content in the composites was determined by thermogravimetric analysis (TGA). The obtained S/C composites (90 wt.%) were then mixed with PVDF binder (10 wt.%) in NMP to form homogeneous slurries. S/C cathodes were fabricated by casting the slurry on a carbon-coated aluminum foil (MTI Corp., USA) and then vacuum-dry overnight at 70 °C. When considering the mass of modification materials, the actual sulfur content of sulfur cathodes was calculated to be 52 wt.%. The sulfur loading was controlled at about 1.4 mg cm^{-2} for regular electrochemical measurements. Cathodes with high sulfur loading of 4.0 mg cm^{-2} have also been investigated to demonstrate the practical application of MFLC-modified separators for Li-S batteries.

2.4. Visualized Li_2S_6 adsorption

Li_2S_6 as nominal stoichiometry was chosen as a representative of polysulfides. A Li_2S_6 solution (10 mmol L^{-1}) was prepared as follows:

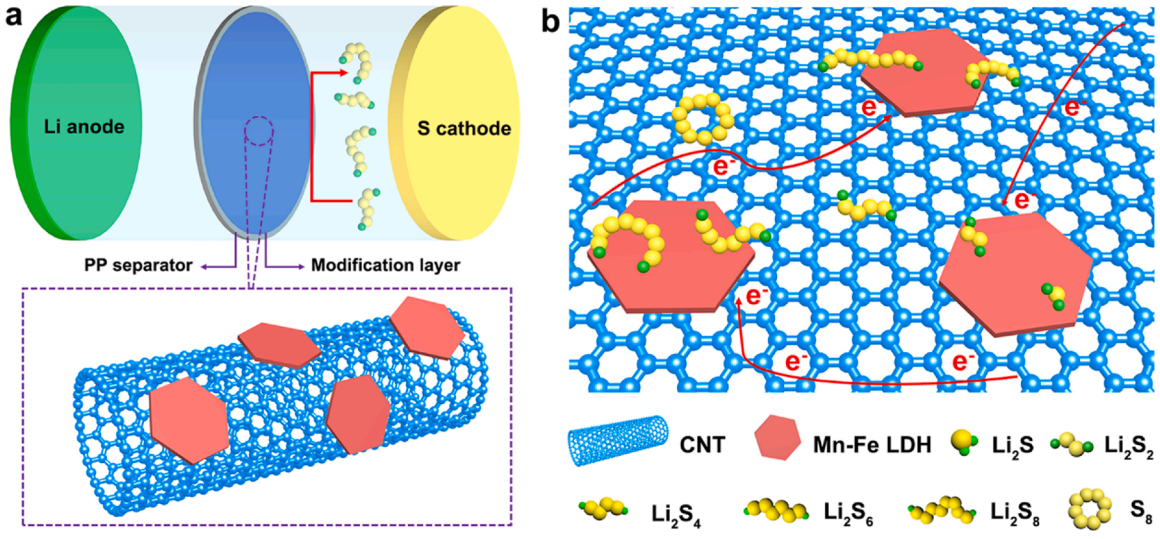

Fig. 1. (a) Schematic representation of MFLC-modified separators used in Li-S batteries. (b) Adsorption and conversion of sulfur species on MFLC.

Li_2S and S were mixed with a molar ratio of 1:5 and then added to the equal volume of 1,3-dioxolane and 1,2-dimethoxyethane under vigorous stirring for 24 h. CNT, Mn-Fe LDH, and MFLC were added to the as-prepared Li_2S_6 solution separately for adsorption measurements. A pure Li_2S_6 solution was used as a control experiment. The color change of the Li_2S_6-adsorbed solutions was compared with the pure solution to determine the adsorption. All procedures were conducted in an Ar-filled glove box.

2.5. Li_2S_6/MFLC composite materials for XPS

Yellow Li_2S_6 powder was obtained from the Li_2S_6 solution by washing with toluene and vacuum drying. To synthesize the Li_2S_6/MFLC composite for the X-ray photoelectron spectroscopy (XPS) study, MFLC powder (20 mg) was added to the Li_2S_6 solution (5.0 mL). The mixture was vigorously stirred to realize sufficient adsorption. The precipitated product was centrifuged and vacuum dried for the XPS measurement. All procedures were conducted in an Ar-filled glove box.

2.6. Materials characterization

The materials crystal structure was examined by X-ray powder diffractometer (Rigaku) using monochromatic Cu Kα radiation (λ = 1.5406 Å). The morphology and structure were characterized by scanning electron microscope (SEM, Philips/FEI XL 40 FEG) and transmission electron microscope (TEM, JEOL-JSM-2100) at an accelerating voltage of 200 kV. An energy-dispersive X-ray Spectroscope (EDS) attached to the SEM instrument was employed to analyze the sample composition. Elemental mapping images were recorded using the EDS spectroscope attached to TEM. Thermogravimetric analysis (TGA, Pvris Diamond) was carried out under a flow of N_2 using a heating rate of 10 °C min^{-1}. Raman spectra were collected on an HR 800 Raman spectroscope (J Y, France) equipped with a synapse charge-coupled device (CCD) detector and confocal Olympus microscope. The spectrograph uses 600 g mm^{-1} gratings and a 633 nm He-Ne laser. X-ray photoelectron spectroscopy (XPS) measurements were carried out with a K-alpha XP spectrometer (Thermo Scientific), equipped with a monochromatic X-ray source (Al Kα = 1486.6 eV).

2.7. Electrochemical measurements

2032 coin-type cells (MTI Corp., USA) were assembled with S/C cathodes, metallic Li foil (Sigma-Aldrich) anodes, and modified or bare PP separators. 1 M lithium bis(trifluoromethanesulfonyl) imide (LiTFSI) in 1,3-dioxolane (DOL) and 1,2-dimethoxyethane (DME) (v/v = 1:1) with 2 wt.% $LiNO_3$ additive was employed as an electrolyte. The electrolyte amount for each cell corresponds to the sulfur content of the cathodes. The electrolyte/sulfur ratio was controlled to be 20 μL mg^{-1} in coin cells. Cell assembly was carried out in an argon-filled glovebox with moisture and oxygen concentration below 5 ppm. Galvanostatic cycling measurements were performed with an M2300 galvanostat (Maccor, Tulsa, USA) in the voltage range of 1.7–2.8 V. Cyclic voltammetry (CV) measurements were performed with an Autolab potentiostat in the voltage range of 1.7–2.8 V at a scan rate of 0.1 mV s^{-1}. Electrochemical impedance spectroscopy (EIS) was carried out in the frequency range from 0.1 Hz to 200 kHz using an Autolab potentiostat. The applied current was based on the weight of pure sulfur (1 C = 1675 mA g^{-1}), and the specific capacities were calculated based on the sulfur mass.

2.8. Assembly of symmetric cells

Symmetric cells were fabricated using MFLC as electrode materials. Bare PP membranes acted as battery separators. A Li_2S_6 solution was added to the electrolyte as active materials to investigate the redox process of sulfur species by the symmetric electrodes. The specific electrode details are as follows: 90 wt.% MFLC mixed with 10 wt.% PVDF binder were dispersed in NMP. The formed slurries were coated on a carbon-coated aluminum foil. The mass loading of MFLC electrodes was about 0.5 mg cm^{-2}. Two identical MFLC electrode disks were used as cathode and anode with bare PP separators for assembling symmetric cells, in which 40 μL electrolyte, containing 0.2 M Li_2S_6 and 1 M LiTFSI in a mixture of DOL and DME (v/v = 1:1) were used. Also, CNT symmetric cells were fabricated using the same method except for using CNT as electrode materials. CV measurements of symmetric cells were performed at a scan rate of 5 mV s^{-1} in the voltage range from −1 to 1 V.

2.9. Li_2S nucleation measurements

A Li_2S_8 solution (0.2 mol L^{-1}) was prepared by adding Li_2S and sulfur with a molar ratio of 1:7 in tetraglyme with 0.5 M LiTFSI supporting electrolyte, which was used as catholyte for the investigations of the nucleation and growth of Li_2S. Carbon fiber paper (CP) was used as a current collector to load MFLC and CNT (2.0 mg cm^{-2}) to fabricate the cathodes. Coin cells were assembled with a cathode and a lithium foil anode separated by a PP membrane. 25 μL Li_2S_8 was dropped onto the cathode and then 25 μL blank electrolyte without Li_2S_8 onto the lithium anode. The cell was first galvanostatically discharged to 2.06 V at a current of 0.112 mA to consume most long-chain polysulfides (Li_2S_8/L_2S_6). It was then potentiostatically controlled at 2.05 V to investigate the Li_2S nucleation and growth until the current dropped to 0.01 mA. The capacity related to the Li_2S deposition was calculated based on current integration, considering Faraday's law.

2.10. Ionic conductivity

The ionic conductivity of MFLC, CNT, and bare PP separators was determined by EIS. Each separator was sandwiched between two stainless steel electrodes with the electrolyte in the coin cells. The ionic conductivity was calculated based on

$$\sigma = l/(R_b A) \tag{1.1}$$

where σ is the ionic conductivity, l represents the thickness of the separator, R_b is the bulk resistance determined by EIS, and A is the area of each stainless steel electrode.

2.11. Lithium-ion transference number

The lithium-ion transference number was determined by chronoamperometry with a constant step potential of 10 mV. MFLC, CNT, and bare PP separators were sandwiched between two lithium metal electrodes in coin cells. The lithium-ion transference number (t_{Li+}) of the cells with different separators can be calculated from the ratio of the steady-state current (I_s) and the initial current (I_o) in the potentiostatic measurements, according to [17]

$$t_{Li+} = I_s/I_o \tag{1.2}$$

3. Results and discussion

Due to the macroporous structure of traditional PP separators shown in the scanning electron microscopy (SEM) image of Fig. 2a, soluble polysulfides can freely migrate through the pores. The resulting erosion of lithium anodes and polysulfide shuttling will inevitably cause capacity losses of sulfur cathodes. After introducing an MFLC modification layer, the SEM image of Fig. 2**b** indicates that the pores of PP separators are now fully covered. The shuttling of polysulfides can therefore be effectively suppressed. The SEM image of pure CNT in Fig. 2**c** reveals a smooth surface. In contrast, after incorporating Mn-Fe LDH, the high-magnification SEM image of the MFLC hybrid material (Fig. 2d) shows much coarser carbon walls. This feature can be ascribed to the grown

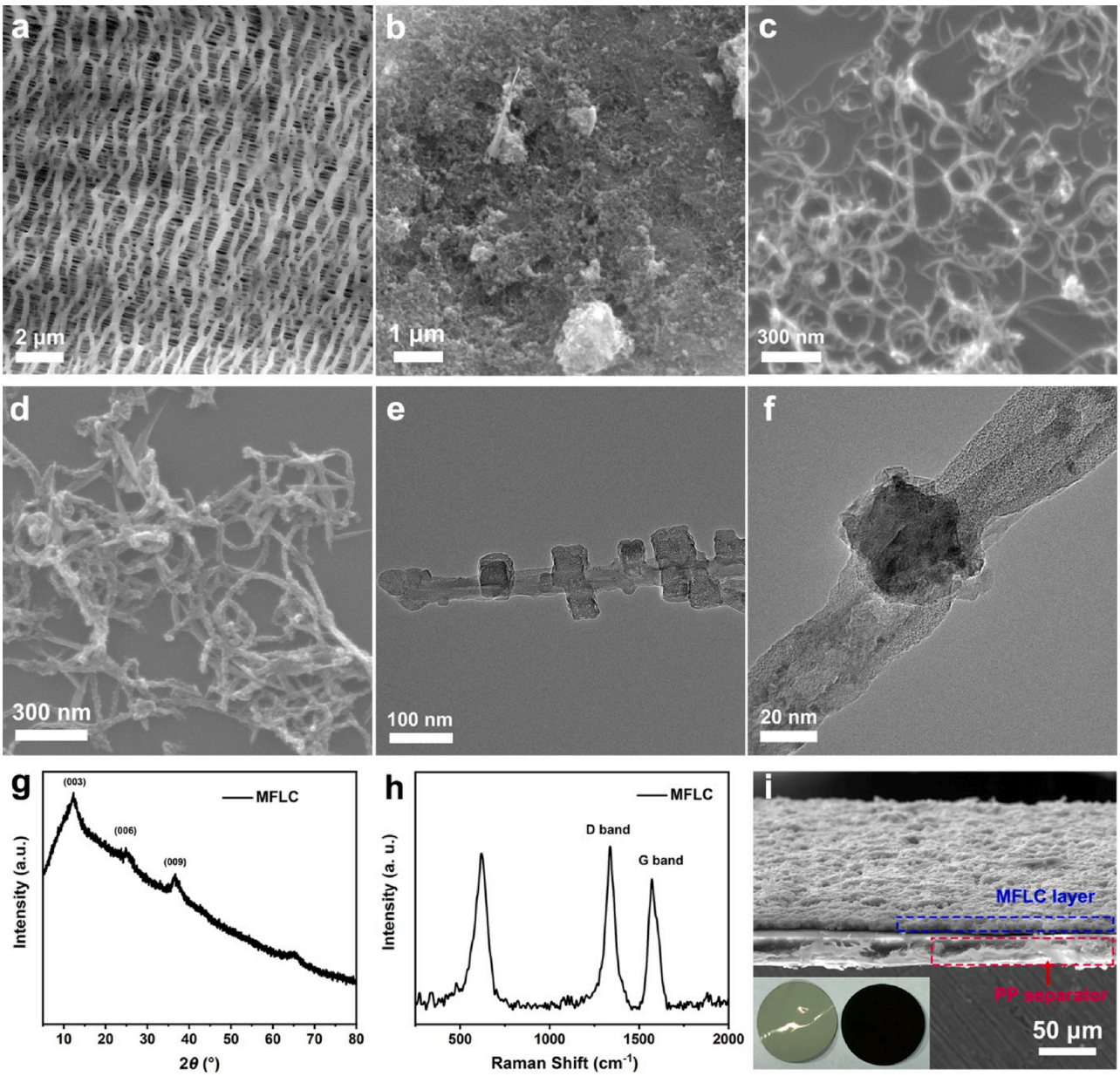

Fig. 2. SEM images of (a) the bare PP separator and (b) MFLC-modified separator. SEM images of (c) pure CNT and (d) MFLC. (e, f) TEM images of MFLC. (g) XRD pattern and (h) Raman spectrum of MFCL. (i) Cross-section of the MFLC-modified separator (inset is the photographs of the MFLC-modified separator, in which left is the backside and right is the modification layer).

Mn-Fe LDH nanosheets onto the CNT. The transmission electron microscopy (TEM) image of Fig. 2**e** clearly demonstrates that many Mn-Fe LDH nanosheets are uniformly decorated at the surface of CNT. Typical size of about 50 nm can be observed in Fig. 2**f**. The large surface area of CNT enables Mn-Fe LDH nanosheets to enlarge the number of polar sites, which are essential to anchor polysulfides. The X-ray diffraction (XRD) pattern in Fig. 2**g** reveals the characteristic peaks of the LDH phase [38]. The D and G bands at 1340 and 1570 cm^{-1} observed in the Raman spectrum of MFLC (Fig. 2h) correspond to the disordered and graphited structures in the carbonaceous material, respectively, which can be ascribed to the presence of CNT. In addition, the band at 617 cm^{-1} can be associated with the Mn-Fe LDH [39]. The EDS analyses (**Fig. S1**) are also consistent with the composition of MFLC, as indicated by the elements of Mn, Fe, O, and C. The compact stacking of MFLC at the PP membrane can be clearly discerned in the cross-section SEM image of Fig. 2**i**. Compared to the PP separator with 25 μm thick, the coated MFLC layer reveals a thickness of only 9 μm. As shown in the inset of Fig. 2i, the MFLC-modified separators preserve the intact structure of the PP membranes (left). The MFLC layer is uniformly coated at the PP separator and does not reveal any cracks (right).

To examine the suppression of polysulfide shuttling by the separators, the MFLC, CNT, and bare PP separators were subject to the polysulfide permeation tests using H-type permeation devices to observe the polysulfide diffusion visually. The Li_2S_6 solution dissolved in DME/DOL (v/v = 1:1) and blank solvent were separated by MFLC, CNT, and bare PP separators, respectively (**Fig. S2**). Li_2S_6 was unable to permeate through the MFLC-modified separator to the other tube within a period of 12 h, implying the effective confinement towards polysulfides. By contrast, the Li_2S_6 permeation was significant for both the CNT and bare PP separators, as revealed by an apparent color change in the right tubes after 12 h. These results demonstrate that the MFLC-modified separator can effectively inhibit the diffusion of polysulfides for high-performance Li-S batteries.

The electrochemistry of Li-S batteries involves a series of

complicated redox reactions. To determine whether MFLC materials improve the redox kinetics for polysulfides, symmetric cells using identical MFLC electrodes and Li_2S_6 solution as electrolyte were assembled to evaluate the redox conversion of polysulfides. Cyclic voltammetry (CV) measurements were performed to characterize the redox reaction of Li_2S_6 in this symmetric cell. From the CV curves in Fig. 3**a** and **b**, the cells without Li_2S_6 solution only reveal low capacitive currents (dashed lines). With the addition of the Li_2S_6 solution, distinct redox peaks can be observed from the MFLC electrode configuration at −0.25 and 0.25 V, respectively, implying the reduction of Li_2S_6 to Li_2S_2/Li_2S and the reverse reaction during oxidation [40,41]. The Li_2S_6 symmetric cell using the MFLC electrodes (Fig. 3a) reveals a significantly higher current response than the one with CNT electrodes (Fig. 3b). The enhanced current response originates from the accelerated redox reactions of Li_2S_6, occurring at the electrolyte/electrode interface. These CV results indicate that MFLC significantly accelerates the redox conversion of polysulfides compared to CNT.

EIS of symmetric cells also validates the accelerated charge transfer kinetics. As shown in Fig. 3c, the Nyquist plot of the pristine cell with MFLC symmetric electrodes reveals a significantly decreased semicircle, indicating smaller charge transfer resistance (R_{ct}) than its CNT counterpart. The resulting EIS equivalent circuit with fitting results is presented in **Fig. S3** and **Table S1**. The introduction of Mn-Fe LDH effectively improves charge transfer, contributing to enhanced redox kinetics of sulfur cathodes.

To further demonstrate the accelerated liquid-solid conversion of sulfur species by MFLC, Li_2S potentiostatic deposition experiments have been performed [42]. The designed cell configuration is shown in **Fig. S4**. Li_2S_8 tetraglyme catholyte was employed for the Li_2S deposition on the carbon fiber paper (CP) loaded MFCL and CNT. Since the limited solubility of sulfur species in the electrolyte, the earlier precipitation of Li_2S may happen due to the concentrated polysulfides accumulating in the cathode region. This polysulfide concentration effect may mix with the acceleration deposition of Li_2S by MFLC, which might be challenging to distinguish them. In this cell configuration, all the starting chemical components are the same except for the loaded MFCL and CNT. Therefore, it is fair to compare the accelerated effects of MFCL and CNT on the deposition of Li_2S. Cells were initially galvanostatically discharged to 2.06 V to consume most long-chain polysulfides (Li_2S_8/L_2S_6), followed by potentiostatic discharging at 2.05 V (a critical overpotential of 10 mV to provide a driving force for the nucleation of Li_2S) to drive the formation of Li_2S. The corresponding potentiostatic discharge curves of MFCL and CNT are shown in Fig. 3**d** and **e**. Different colors indicate the capacity contributions of Li_2S_8/L_2S_6 reduction and the deposition of Li_2S. Obviously, MFLC shows a stronger current response towards the Li_2S deposition than CNT. The capacity related to the Li_2S deposition on MFCL is determined to be 192 mA h g^{-1}, which is higher than that on CNT (76 mA h g^{-1}). These results clearly indicate that the MFCL electrode shows the higher activity towards Li_2S deposition, implying accelerated liquid-solid conversion of sulfur species by MFCL.

The migration of lithium ions through the separator is critical to the mass-transport properties of the battery system. Therefore, the ionic conductivity of the modified separators in the electrolyte has been investigated by EIS using two stainless steel electrodes. The Nyquist plots shown in Fig. 3**f** reveal that the MFLC separators have a smaller resistance than the CNT-based separator, the latter being very similar to bare PP separators. The calculated ionic conductivity of MFLC separators (0.7 mS cm^{-1}) is higher than that of bare separators (0.57 mS cm^{-1}), indicating the good transport pathways for lithium ions. In addition, the lithium-ion transference numbers have been investigated for the three separators. Based on the current-time curves shown in **Fig. S5**, the MFLC separators exhibit a higher lithium-ion transference number (0.61) than that for CNT (0.43) and bare PP separators (0.58), suggesting better lithium-ion transport.

To evaluate the improved sulfur utilization by MFLC, coin-type cells composed of metallic Li anodes, sulfur/carbon (S/C) composite cathodes, and MFLC-modified separators have been assembled to determine the electrochemical performance. Cells using CNT-modified and bare PP separators were also evaluated for comparison. The sulfur content in the composites was determined to be 70 wt.% by TGA in **Fig. S6**. The cycling performance of Li-S batteries with different separators is evaluated at 0.2 C rate. As shown in Fig. 4**a-c**, all three batteries exhibit two clear

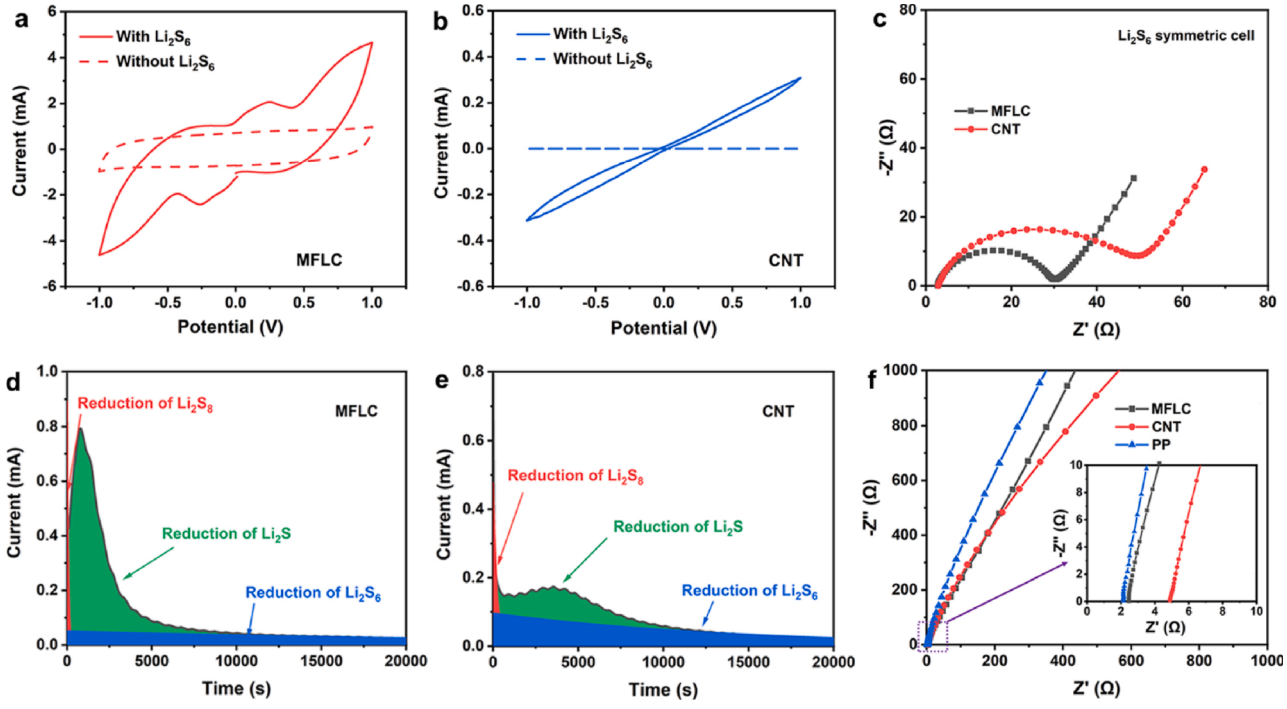

Fig. 3. CV curves of the Li_2S_6 symmetric cells using identical (a) MFLC and (b) CNT electrodes. (c) Nyquist plots of pristine Li_2S_6 symmetric cells with identical MFLC and CNT electrodes. Potentiostatic discharge curves of (d) MFLC and (e) CNT cathodes with the Li_2S_8 tetraglyme catholyte at 2.05 V. (f) Nyquist plots estimating the ionic conductivity of MFLC, CNT, and PP separators.

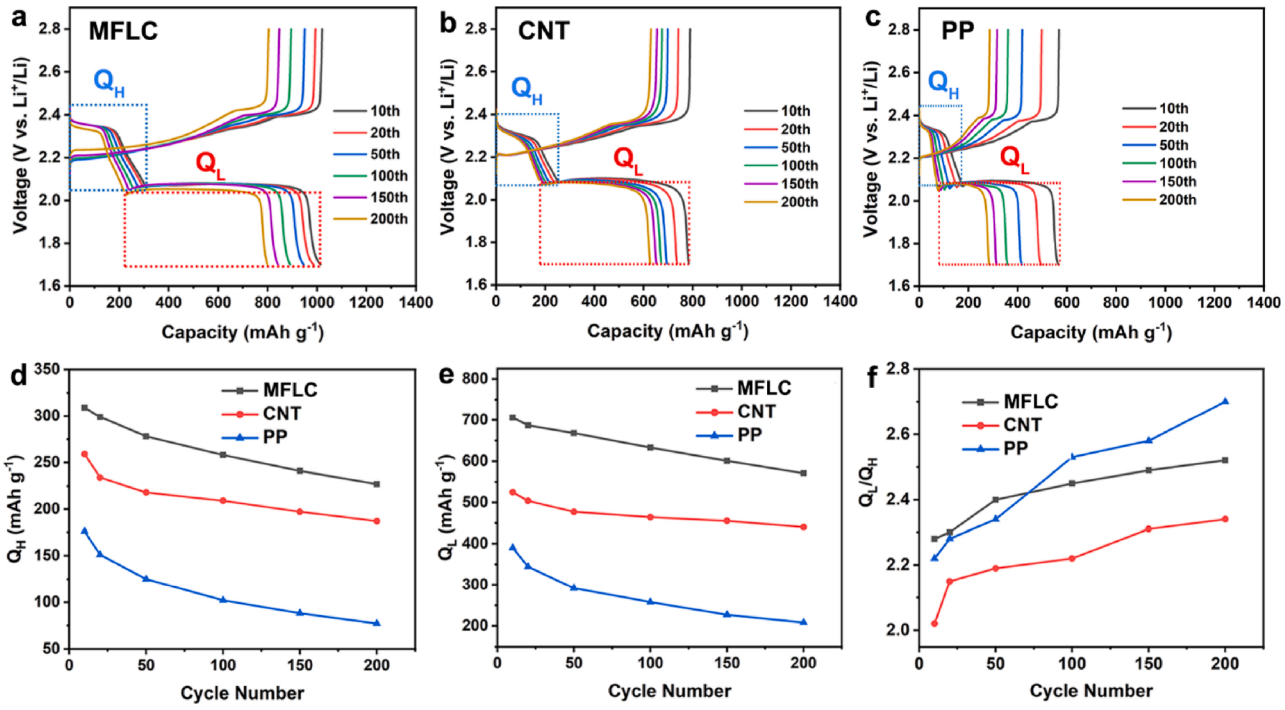

Fig. 4. Voltage profiles of Li-S batteries with (a) MFLC, (b) CNT, and (c) PP separators at 0.2 C at various indicated cycles. (d) Corresponding high-voltage plateau capacities (Q_H), (e) low-voltage plateau capacities (Q_L), and (f) the ratio of Q_L to Q_H of three batteries.

voltage plateaus during discharging, representing the redox reactions between metallic lithium and sulfur. These are the typical electrochemical characteristics of Li-S batteries. Cells with the MFLC-modified separators show the highest storage capacity and capacity retention, indicating efficient sulfur utilization during cycling.

As the discharging curves of Li-S batteries reveal well-defined voltage plateaus, the change in voltage discharge plateaus can distinctly reflect the electrochemical reaction performance of the sulfur cathodes. Therefore, the two plateaus are extracted from the discharging voltage profiles to analyze the sulfur utilization. The capacity from the high-voltage plateau (Q_H) indicates the reduction process from elemental sulfur to soluble polysulfides (Li_2S_n, $4 \leq n \leq 8$) at the cathode. In contrast, the low-voltage plateau capacity (Q_L) represents the continuing reduction at the cathode from soluble polysulfides to insoluble sulfides (Li_2S_n, $n = 1, 2$) [43]. The high-voltage plateau is associated with the formation of soluble polysulfides, which may result in polysulfide diffusion and induce the well-known shuttle effect. If polysulfides, which are produced continuously in the high-voltage plateau, can effectively be anchored within the cathode, a higher Q_H is to be expected. Q_H, therefore, indicates the confinement capability of polysulfides by the modified separators. The low-voltage plateau involves the reduction from soluble polysulfides to insoluble Li_2S_2/Li_2S, resulting in a sluggish charge transfer. An accelerated redox reaction in this stage can contribute to improved plateau capacity. Q_L, therefore, reflects the redox reaction process of sulfur species. Investigating the change in Q_H and Q_L during cycling makes it possible to evaluate the anchoring and conversion of sulfur species. The theoretical capacities of Q_H and Q_L are 419 and 1256 mA h g^{-1}, respectively [44].

Fig. 4**d** and **e** show the Q_H and Q_L of Li-S batteries with the MFLC, CNT, and bare PP separators at 0.2 C as a function of cycle number. The values of Q_H and Q_L are also listed in **Table S2.** Both Q_H and Q_L of the MFLC-modified separator delivered higher capacities than the other electrodes. The battery with bare PP separators reveals a Q_H of 176 mA h g^{-1} after 10 cycles, which is further reduced to 77 mA h g^{-1} after 200 cycles. This indicates that soluble polysulfides consistently diffuse from sulfur cathodes into the electrolyte and is no longer available for electrochemical reactions. After introducing a CNT modification layer onto the PP membrane, an improvement in Q_H can be seen, indicating the partial confinement of polysulfides by CNT. By contrast, the MFLC-modified separator achieved a Q_H of 309 mA h g^{-1} after 10 cycles while maintaining 227 mA h g^{-1} over 200 cycles. These results indicate that MFLC-modified separators effectively inhibit the diffusion of soluble polysulfides by confining them at the cathode side, implying that abundant polysulfides will be available in the low-voltage plateau. It can be concluded that Q_H plays a critical role in the overall performance of sulfur cathodes. The effective confinement of the generated polysulfides in the high-voltage plateau is a prerequisite for the enhanced sulfur utilization. A high Q_H indicates that adequate polysulfides can be afforded for the following liquid-solid conversion reaction in the low-voltage plateau. Together with the good electrochemical charge transfer kinetics, a high Q_L also can be achieved.

Among the three battery configurations, the MFLC-modified separator batteries also show the highest Q_L value upon cycling (Fig. 4e), which can be attributed to the enhanced redox conversion of sulfur species. Compared to CNT modification layers, the introduction of Mn-Fe LDH not only inhibits the shuttling problem of the polysulfides but also accelerates their conversion during cycling. These results correspond with the Li_2S_6 symmetric cell analyses. Such an improved utilization of sulfur species can be validated by the Q_L/Q_H ratio. From the theoretical capacities of Q_L and Q_H, a theoretical value for Q_L/Q_H of 3 is expected. As shown in Fig. 4f, all three separators show values below 3, indicating that the formed polysulfides in the high-voltage plateau cannot fully convert to lithium sulfides in the low-voltage plateau region. The MFLC-modified separators reveal higher Q_L/Q_H ratios than CNT during the cycling experiment, which means that the conversion of polysulfides to insoluble lithium sulfides is enhanced.

Interestingly, bare PP separators show higher Q_L/Q_H ratios than CNT and even exceed MFLC at higher cycle numbers. This fact may result from the macroporous property of the PP membrane. Due to the micrometer pore size, the PP separators can barely inhibit the diffusion of polysulfide molecules into the electrolyte. As cycling continues, an increasing amount of polysulfides generated on the high-voltage plateau will diffuse away from the cathode and accumulate in the electrolyte. These dissolved polysulfides may not entirely convert to sulfur during

charging and then participate in the discharge process during the subsequent cycling. Therefore, they will provide the extra discharge capacity in the low-voltage plateau region, leading to a higher Q_L and higher Q_L/Q_H ratios at the higher cycle numbers for the PP separators.

Benefiting from the advantages of MFLC, Fig. 5**a** shows that the cells with MFLC-modified separators delivered the highest initial capacity of 1138 mA h mg^{-1} at 0.2 C. Favorable capacity retention of 70 % was achieved over 200 cycles with a Coulombic efficiency of more than 99 %, implying good sulfur utilization and electrode stability. By contrast, the cells with PP separators delivered only 285 mA h g^{-1} after 200 cycles, with a poor capacity retention of only 35.4 %. Although the shuttling of polysulfides was partially inhibited by introducing a CNT modification layer, the cells with CNT-modified separators still incurred a considerable capacity fading upon cycling, resulting in a low capacity of 626 mA h g^{-1} after 200 cycles. To further demonstrate the effective suppression of the shuttling of polysulfides by the MFLC separator, the MFLC, CNT, and PP separators have been checked after disassembling the cycled coin cells (**Fig. S7**). The MFLC and CNT separators facing the cathodes did not exhibit any color changes, indicating no sulfur species were deposited on the separators. By contrast, significant yellow spots were observed at the surface of the bare PP separator. These color distinctions demonstrate that the diffusion of polysulfides has been successfully inhibited by MFLC-modified separators, which is consistent with the corrosion of the cycled lithium anodes. As shown in Fig. 5b, the lithium anode with MFLC-modified separators reveals a smooth and homogeneous morphology even after 200 cycles. In contrast, the one with a PP separator (Fig. 5c**)** indicates many cracks due to the detrimental reaction of polysulfides with lithium.

Moreover, the effective suppression of polysulfide shuttling can also be determined by the battery self-discharge behavior. The cell with MFLC-modified separators reveals a stable open-circuit voltage of 2.4 V, which is higher than the voltages attained for the cells with CNT and bare PP separators after a resting period 50 h following 50 cycles (Fig. 5d). This behavior indicates the effective inhibition of the battery self-discharge by the MFLC-modified separators.

Besides, the CV curves of the cells with MFLC-modified separators shown in Fig. 5**e** demonstrate favorable electrochemical reversibility of the sulfur cathode, suggested by well-preserved profiles during the initial cycles, revealing only minor changes. Typical Li-S electrochemical characteristics can be concluded from these CV curves. Two cathodic peaks located at about 2.32 and 2.03 V are associated with the conversion from sulfur to polysulfides at the cathode (Li_2S_n, $4 \leq n \leq 8$) and insoluble sulfides (Li_2S_n, $n = 1, 2$), respectively. The corresponding two anodic peaks indicate the reversible oxidation reactions from the

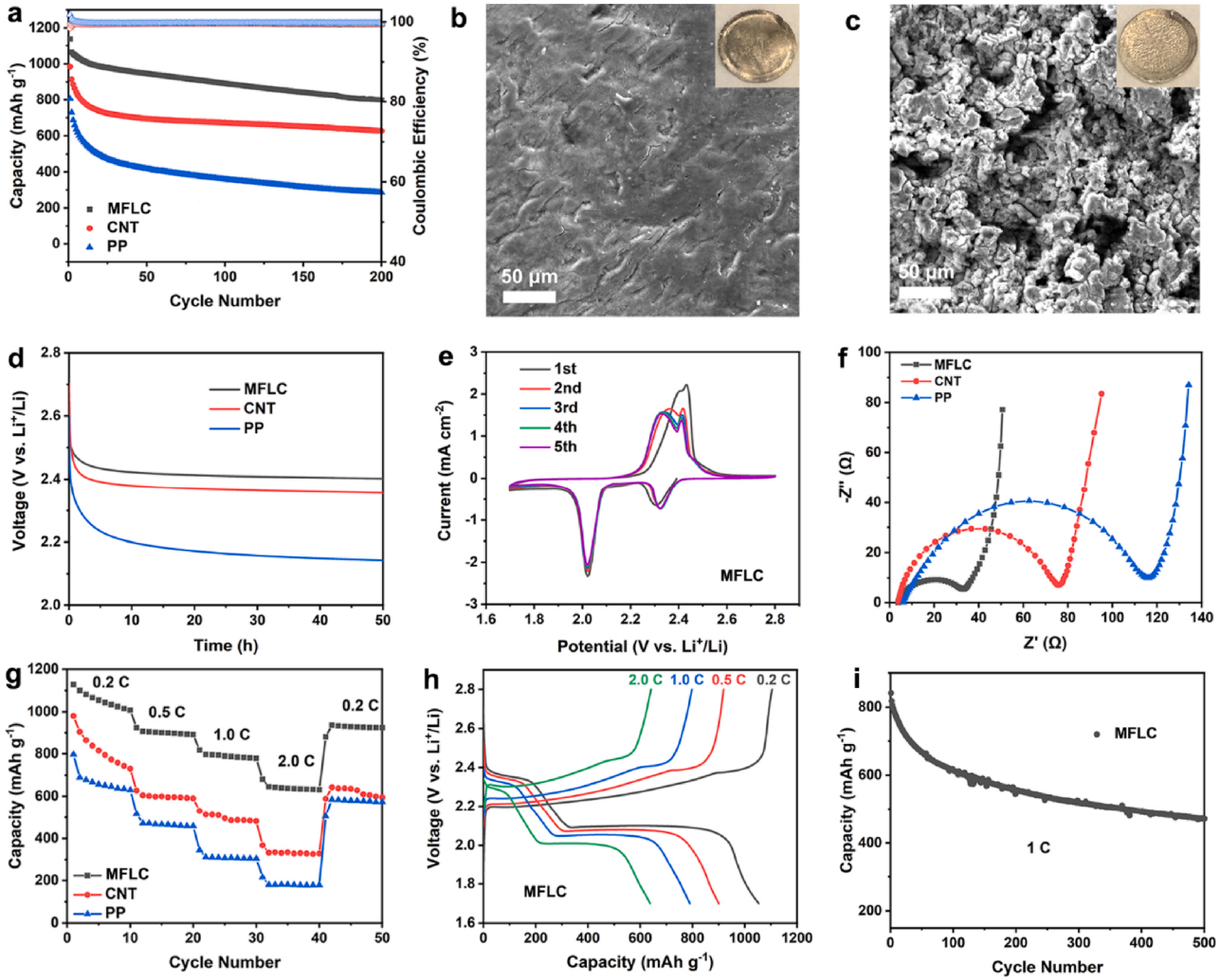

Fig. 5. (a) Cycling performance of Li-S batteries with MFLC, CNT, and PP separators at 0.2 C. SEM images of the cycled lithium anodes with (b) MFLC and (c) PP separators (Insets show the corresponding photographs). (d) Self-discharge behavior of cells with MFLC, CNT, and PP separators after a resting period of 50 h following 50 cycles. (e) CV curves of Li-S batteries with MFLC separators in the initial five cycles. (f) Nyquist plots of the Li-S cells with MFLC, CNT, and PP separators. (g) Rate capabilities of Li-S batteries with three separators at various current densities from 0.2 to 2 C. (h) Voltage profiles of Li-S batteries with MFLC separators at various indicated rates. (i) Prolonged cycling performance of Li-S batteries with MFLC separators at 1 C.

sulfides to polysulfides and finally back to elemental sulfur. The two well-defined anodic peaks after the first cycle indicate good reaction kinetics of Li-S batteries. The CV results are in good agreement with the voltage profiles of Fig. 4**a**. The CV curves of the cells with MFLC, CNT, and bare PP separators will be further discussed to reveal the enhanced redox kinetics of the sulfur cathodes (**Fig. S8**). Compared to CNT and bare PP separators, MFLC revealed stronger CV peak intensities, implying enhanced sulfur cathode utilization. The second cathodic peak and onset potential of MFLC exhibited a more positive shift, indicating accelerated liquid-solid conversion from polysulfides to Li_2S. The subsequent anodic peak and onset potential of MFLC, corresponding to the reverse liquid-solid reaction process, shifted towards more negative voltages. Consequently, MFLC shows accelerated sulfur conversion upon cycling. These results are consistent with the Li_2S_6 symmetric cell tests and the Li_2S deposition experiments described in Fig. 3. The EIS measurements also reveal the enhanced redox kinetics of the sulfur cathodes induced by the MFLC-modified separators. **Table S3** presents the corresponding fitting results. From the Nyquist plots in Fig. 5f, the cell with MFLC-modified separators exhibits the smallest R_{ct} among the three cell configurations, indeed indicating accelerated charge transfer.

Cells with MFLC-modified separators display good rate capabilities, as indicated in Fig. 5**g** and **h**. MFLC delivered higher capacities from 0.2 to 2 C than CNT and PP. Stable capacities of 1043 (0.2 C), 898 (0.5 C), 789 (1.0 C), and 637 mA h g^{-1} (2.0 C) were achieved. When the current density turned back to 0.2 C, MFLC still maintained a reversible capacity of 927 mA h g^{-1}. By contrast, the CNT and PP cells suffered heavy capacity decay with the current density increasing, only delivering capacities of 334 and 179 mA h g^{-1} at 2.0 C. The accelerated electrode kinetics by MFLC can also be confirmed by the voltage profiles at various current densities, in which two well-defined discharge voltage plateaus remained (Fig. 5h). The prolonged cycling test of the cells with MFLC-modified separators was carried out at 1.0 C. As shown in Fig. 5i, MFLC delivers a reversible capacity of 471 mA h g^{-1} after 500 cycles with a capacity fading of only 0.088 % per cycle, almost three times higher than typical nickel manganese cobalt oxide (NMC) cathode materials. **Table S4** summarizes the reported results using various separator modification layers and interlayer materials for Li-S batteries. MFLC-modified separators exhibit competitive electrochemical performance compared to the previous reports. These results firmly demonstrate the structural advantages of MFLC on enhancing sulfur utilization for stable and long-life Li-S batteries.

To explore the practical applications of MFLC-modified separators for Li-S batteries with high energy density, cells employing MFLC-modified separators with a high sulfur loading of 4.0 mg cm^{-2} were further assessed. **Fig. S9** presents the resulting voltage profiles upon cycling at 0.2 C. The high loading cathode with MFLC-modified separators initially delivered a high capacity of 994 mA h g^{-1}. It maintained a steady capacity of 715 mA h g^{-1} after 100 cycles. The increase in sulfur loading barely incurs heavy polarization, implying good sulfur utilization and cycling stability. Compared to the cathodes with low sulfur loading, cathodes with high sulfur loading reveal a relatively decreased capacity at 0.2 C. This feature is explained by the increased thickness of high sulfur loading cathodes, so that the overall electrode reaction of sulfur may not be adequate. However, even for high sulfur loadings of 4 mg cm^{-2} (**Fig. S9**), the batteries with MFLC-modified separators also exhibit better cycling performance than the batteries with bare PP separators with a low sulfur loading of 1.4 mg cm^{-2} (Fig. 5a, blue line). Therefore, these results indicate that the MFLC-modified separators show good application potentials for practical Li-S batteries.

Effective suppression of the polysulfide diffusion is critical for increasing the sulfur electrode utilization. Visualized polysulfide adsorption experiments present a straightforward understanding of the interaction between polysulfides and MFLC. As shown in Fig. 6a, an equal amount of CNT, Mn-Fe LDH, and MFLC were respectively added to

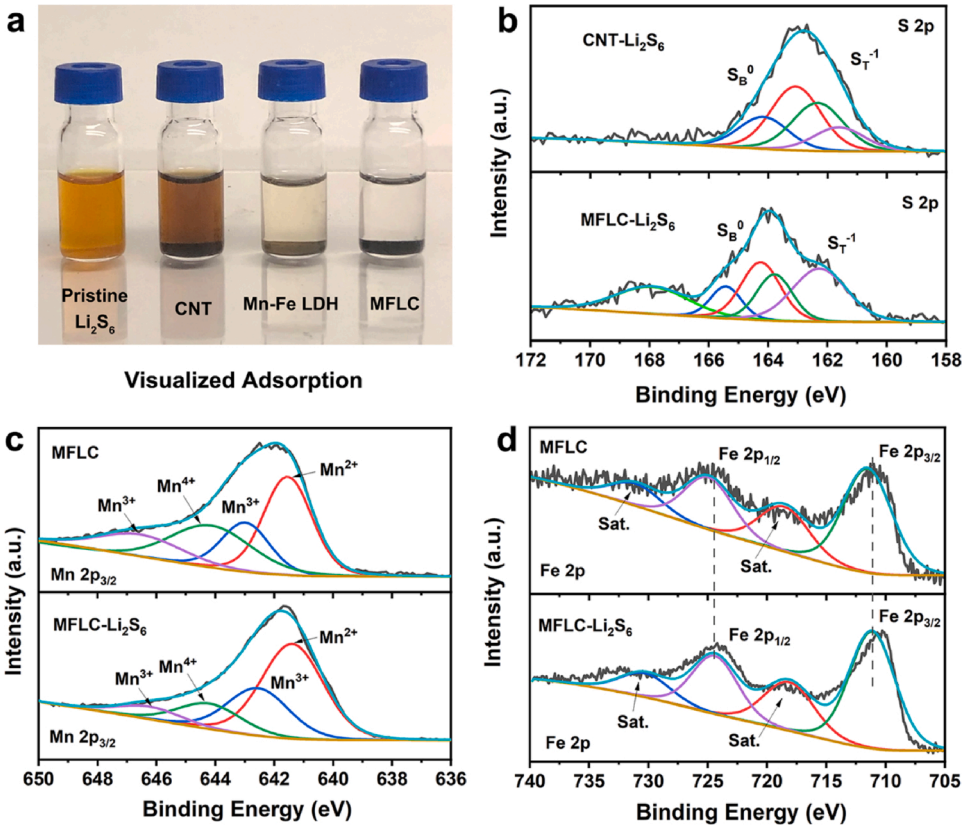

Fig. 6. (a) Visualized Li_2S_6 adsorption of CNT, Mn-Fe LDH, and MFLC. (b) High-resolution S 2p XPS spectra of CNT-Li_2S_6 and MFLC-Li_2S_6. (c) Mn $2p_{3/2}$ spectra of MFLC and MFLC-Li_2S_6. (d) Fe 2p spectra of MFLC and MFLC-Li_2S_6.

a Li_2S_6 solution in order to investigate the adsorption process. The Li_2S_6 solution containing Mn-Fe LDH and MFLC turned almost transparent, whereas the one with CNT still maintained the initial yellow solution. These results indicate that the introduction of MnFe-LDH clearly enhances the interaction with polysulfides, implying that the shuttle problem of polysulfides can indeed be inhibited via effective anchoring of sulfur species by Mn-Fe LDH.

Such interaction has been further investigated by XPS. The Li_2S_6 adsorbed CNT and MFLC, accordingly denoted as CNT-Li_2S_6 and MFLC-Li_2S_6, were dried for the XPS studies. As shown in Fig. 6b, the S 2p spectrum of CNT-Li_2S_6 displays two doublets at 161.6/162.3 and 163.1/164.2 eV, which can be associated with the terminal sulfur (S_T^{-1}) and bridging sulfur (S_B°), respectively [45]. The S 2p spectrum of CNT-Li_2S_6 exhibits the same binding energies as pristine Li_2S_6 (**Fig. S10**), suggesting the absence of any interaction between CNT and Li_2S_6. This observation is consistent with the visualized adsorption, where CNT failed to absorb polysulfides (see second CNT tube in Fig. 6a). In contrast, the S 2p spectrum of MFLC-Li_2S_6 (Fig. 6b) clearly shifts to higher binding energies, from which the conclusion becomes clear considering the deconvoluted curves. That implies a decrease in the electronic density of the sulfur atoms. Besides, a new peak has emerged at 168 eV, which can be attributed to SO_x species from the partial oxidation of Li_2S_6 by MFLC [46]. The poor solubility of produced SO_x species has been validated to mitigate the polysulfide shuttling effectively.

Furthermore, the Mn 2p and Fe 2p spectra of MFLC-Li_2S_6 are analyzed to determine this interaction in more detail. The Mn $2p_{3/2}$ spectrum of MFLC, shown in the upper graph of Fig. 6c, exhibits a characteristic multiplet. The deconvoluted peaks of Mn $2p_{3/2}$ located in a range of 641.5–646.6 eV suggest contributions from Mn^{2+}, Mn^{3+}, and Mn^{4+} [47]. Compared to MFLC, the Mn $2p_{3/2}$ spectrum of MFLC-Li_2S_6 reveals a higher Mn^{2+} contribution with enhanced peaks, and the Mn^{4+} peaks decrease considerably. These results imply the partial reduction of Mn-Fe LDH, hence resulting in the oxidation of Li_2S_6 to SO_x species, which is well consistent with the S 2p spectrum of MFLC-Li_2S_6 (Fig. 6b). The Fe 2p spectrum of MFLC-Li_2S_6 indicates a decrease in banding energies compared to pure MFLC (Fig. 6d). It can be concluded that the peak change in Mn 2p and Fe 2p spectra of MFLC-Li_2S_6 results from the electron transfer between S atoms of Li_2S_6 and Mn/Fe atoms of Mn-Fe LDH. From the visualized adsorption and XPS analyses, it is clear that the chemical interaction between MFLC and polysulfides significantly suppresses the polysulfide diffusion, leading to the enhanced sulfur utilization for Li-S batteries.

4. Conclusions

In summary, an MFLC hybrid material has been designed as a modification layer on a PP separator to achieve enhanced sulfur utilization for more efficient Li-S batteries. This developed MFLC composite structure combines the high conductivity of CNT with good chemical bonding of Mn-Fe LDH towards polysulfides. The MFLC-modified separator strongly suppresses the diffusion of polysulfides and accelerates their electrochemical charge transfer kinetics. The combined function of MFLC has been demonstrated by XPS measurements, symmetric cell experiments, and discharge voltage plateaus analyses. The results conclude that the effective anchoring of sulfur species on the cathode side is critical for achieving effective sulfur utilization. Specifically, the high discharge capacities observed at the high-voltage plateaus are responsible for efficient sulfur species conversion in the low-voltage plateau. The enhanced sulfur utilization, therefore, can be directly evaluated from the voltage discharge plateaus. As a result, Li-S batteries with an MFLC-modified separator delivered a high initial capacity of 1138 mA h g^{-1} with 70 % capacity preservation after 200 cycles at 0.2 C. These results indicate a new solution for future applications of Li-S batteries and provide a simple approach to determine the efficiency of sulfur utilization.

Declaration of Competing Interest

The authors declare that they have no known competing financial interests or personal relationships that could have appeared to influence the work reported in this paper.

Acknowledgments

The authors L. Zhou, Y. Zhang, and M. Jiang acknowledge the financial support of the China Scholarship Council.

Appendix A. Supplementary data

Supplementary material related to this article can be found, in the online version, at doi:https://doi.org/10.1016/j.mtcomm.2021.102133.

References

[1] J.M. Tarascon, M. Armand, Nature 414 (2001) 359–367.
[2] M. Li, J. Lu, Z. Chen, K. Amine, Adv. Mater. 30 (2018), 1800561.
[3] Z.W. Seh, Y. Sun, Q. Zhang, Y. Cui, Chem. Soc. Rev. 45 (2016) 5605–5634.
[4] Y. Hu, W. Chen, T. Lei, Y. Jiao, J. Huang, A. Hu, C. Gong, C. Yan, X. Wang, J. Xiong, Adv. Energy Mater. 10 (2020), 2000082.
[5] X. Ji, L.F. Nazar, J. Mater. Chem. 20 (2010) 9821.
[6] L. Zhou, D.L. Danilov, R.A. Eichel, P.H.L. Notten, Adv. Energy Mater. (2020).
[7] H.J. Peng, G. Zhang, X. Chen, Z.W. Zhang, W.T. Xu, J.Q. Huang, Q. Zhang, Angew. Chem. Int. Ed. 55 (2016) 12990–12995.
[8] Y. Wang, X. Huang, S. Zhang, Y. Hou, Small Methods (2018), 1700345.
[9] Z. Li, Y. Huang, L. Yuan, Z. Hao, Y. Huang, Carbon 92 (2015) 41–63.
[10] X. Ji, K.T. Lee, L.F. Nazar, Nat. Mater. 8 (2009) 500–506.
[11] M. Yan, H. Chen, Y. Yu, H. Zhao, C.-F. Li, Z.-Y. Hu, P. Wu, L. Chen, H. Wang, D. Peng, H. Gao, T. Hasan, Y. Li, B.-L. Su, Adv. Energy Mater. 8 (2018), 1801066.
[12] J.H. Yun, J.H. Kim, D.K. Kim, H.W. Lee, Nano Lett. 18 (2018) 475–481.
[13] C. Chen, D. Li, L. Gao, P.P.R.M.L. Harks, R.-A. Eichel, P.H.L. Notten, J. Mater. Chem. A 5 (2017) 1428–1433.
[14] X. Liu, J.Q. Huang, Q. Zhang, L. Mai, Adv. Mater. 29 (2017), 1601759.
[15] S.-Y. Li, W.-P. Wang, H. Duan, Y.-G. Guo, J. Energy Chem. (2018).
[16] J. Balach, J. Linnemann, T. Jaumann, L. Giebeler, J. Mater. Chem. A 6 (2018) 23127–23168.
[17] Z.A. Ghazi, X. He, A.M. Khattak, N.A. Khan, B. Liang, A. Iqbal, J. Wang, H. Sin, L. Li, Z. Tang, Adv. Mater. 29 (2017), 1606817.
[18] L. Jiao, C. Zhang, C. Geng, S. Wu, H. Li, W. Lv, Y. Tao, Z. Chen, G. Zhou, J. Li, G. Ling, Y. Wan, Q.H. Yang, Adv. Energy Mater. 9 (2019), 1900219.
[19] J. Guo, Y. Xu, C. Wang, Nano Lett. 11 (2011) 4288–4294.
[20] L. Sun, M. Li, Y. Jiang, W. Kong, K. Jiang, J. Wang, S. Fan, Nano Lett. 14 (2014) 4044–4049.
[21] D. Gueon, J.T. Hwang, S.B. Yang, E. Cho, K. Sohn, D.K. Yang, J.H. Moon, ACS Nano 12 (2018) 226–233.
[22] Q. Pang, D. Kundu, M. Cuisinier, L.F. Nazar, Nat. Commun. 5 (2014) 4759.
[23] S. Mei, C.J. Jafta, I. Lauermann, Q. Ran, M. Kärgell, M. Ballauff, Y. Lu, Adv. Funct. Mater. 27 (2017), 1701176.
[24] F. Wang, X. Ding, R. Shi, M. Li, Y. Lei, Z. Lei, G. Jiang, F. Xu, H. Wang, L. Jia, R. Jiang, Z. Liu, J. Sun, J. Mater. Chem. A 7 (2019) 10494–10504.
[25] L. Zhou, H. Li, X. Wu, Y. Zhang, D.L. Danilov, R.-A. Eichel, P.H.L. Notten, ACS Appl. Energy Mater. 2 (2019) 8153–8162.
[26] Z. Chang, H. Dou, B. Ding, J. Wang, Y. Wang, X. Hao, D.R. MacFarlane, J. Mater. Chem. A 5 (2017) 250–257.
[27] J. Xu, W. Zhang, Y. Chen, H. Fan, D. Su, G. Wang, J. Mater. Chem. A 6 (2018) 2797–2807.
[28] S.-H. Chung, L. Luo, A. Manthiram, ACS Energy Lett. 3 (2018) 568–573.
[29] X. Huang, J. Tang, B. Luo, R. Knibbe, T. Lin, H. Hu, M. Rana, Y. Hu, X. Zhu, Q. Gu, D. Wang, L. Wang, Adv. Energy Mater. 9 (2019), 1901872.
[30] Z. Xiao, Z. Li, X. Meng, R. Wang, J. Mater. Chem. A 7 (2019) 22730–22743.
[31] X. Liang, A. Garsuch, L.F. Nazar, Angew. Chem. Int. Ed. 54 (2015) 3907–3911.
[32] Z. Xiao, Z. Li, P. Li, X. Meng, R. Wang, ACS Nano 13 (2019) 3608–3617.
[33] X. Liang, C. Hart, Q. Pang, A. Garsuch, T. Weiss, L.F. Nazar, Nat. Commun. 6 (2015) 5682.
[34] H. Lin, L. Yang, X. Jiang, G. Li, T. Zhang, Q. Yao, G.W. Zheng, J.Y. Lee, Energy Environ. Sci. 10 (2017) 1476–1486.
[35] Z. Yuan, H.J. Peng, T.Z. Hou, J.Q. Huang, C.M. Chen, D.W. Wang, X.B. Cheng, F. Wei, Q. Zhang, Nano Lett. 16 (2016) 519–527.
[36] J. Zhang, Z. Li, Y. Chen, S. Gao, X.W.D. Lou, Angew. Chem. Int. Ed. 57 (2018) 10944–10948.
[37] H.J. Peng, Z.W. Zhang, J.Q. Huang, G. Zhang, J. Xie, W.T. Xu, J.L. Shi, X. Chen, X. B. Cheng, Q. Zhang, Adv. Mater. 28 (2016) 9551–9558.
[38] Y. Ruan, X. Jia, C. Wang, W. Zhen, X. Jiang, Chem. Commun. 54 (2018) 11729–11732.
[39] Y.-T. Lai, W.-T. Liu, L.-J. Chen, M.-C. Chang, C.-Y. Lee, N.-H. Tai, J. Mater. Chem. A 7 (2019) 3962–3970.

[40] J. Xu, W. Zhang, H. Fan, F. Cheng, D. Su, G. Wang, Nano Energy 51 (2018) 73–82.
[41] J. Qian, F. Wang, Y. Li, S. Wang, Y. Zhao, W. Li, Y. Xing, L. Deng, Q. Sun, L. Li, F. Wu, R. Chen, Adv. Funct. Mater. 30 (2020), 2000742.
[42] F.Y. Fan, W.C. Carter, Y.M. Chiang, Adv. Mater. 27 (2015) 5203.
[43] S. Tu, X. Chen, X. Zhao, M. Cheng, P. Xiong, Y. He, Q. Zhang, Y. Xu, Adv. Mater. 30 (2018), 1804581.
[44] C.-H. Chang, S.-H. Chung, A. Manthiram, J. Mater. Chem. A 3 (2015) 18829–18834.
[45] X. Liang, C.Y. Kwok, F. Lodi-Marzano, Q. Pang, M. Cuisinier, H. Huang, C.J. Hart, D. Houtarde, K. Kaup, H. Sommer, T. Brezesinski, J. Janek, L.F. Nazar, Adv. Energy Mater. 6 (2016), 1501636.
[46] X. Wang, G. Li, J. Li, Y. Zhang, A. Wook, A. Yu, Z. Chen, Energy Environ. Sci. 9 (2016) 2533–2538.
[47] X. Chen, L. Yuan, Z. Hao, X. Liu, J. Xiang, Z. Zhang, Y. Huang, J. Xie, ACS Appl. Mater. Interfaces 10 (2018) 13406–13412.